Environ. Sci. Technol. **1999**, *33*, 713−717

Zinc Ligands in the Metal Hyperaccumulator *Thlaspi caerulescens* As Determined Using X-ray Absorption Spectroscopy

DAVID E. SALT,*,† ROGER C. PRINCE,‡ ALAN J. M. BAKER,§ ILYA RASKIN,∥ AND INGRID J. PICKERING⊥

Chemistry Department, Northern Arizona University, Flagstaff, Arizona 86011, Exxon Research and Engineering, Annandale, New Jersey 08801, Department of Animal and Plant Sciences, University of Sheffield, Sheffield, S10 2TN, U.K., AgBiotech Center, Rutgers University, Cook College, New Brunswick, New Jersey 08903, and Stanford Synchrotron Radiation Laboratory, SLAC, Stanford, California 94309

Using the noninvasive technique of X-ray absorption spectroscopy (XAS), we have been able to determine the ligand environment of Zn in different tissues of the Zn-hyperaccumulator *Thlaspi caerulescens* (J. & C. Presl.). The majority of intracellular Zn in roots of *T. caerulescens* was found to be coordinated with histidine. In the xylem sap. Zn was found to be transported mainly as the free hydrated Zn^{2+} cation with a smaller proportion coordinated with organic acids. In the shoots, Zn coordination occurred mainly via organic acids, with a smaller proportion present as the hydrated cation and coordinated with histidine and the cell wall. Our data suggest that histidine plays an important role in Zn homeostasis in the roots, whereas organic acids are involved in xylem transport and Zn storage in shoots.

Introduction

A number of plant species, particularly in the genus *Thlaspi*, have the unusual ability of accumulating Zn to very high concentrations in their shoots; some species have been recorded with up to 4% of their shoot dry weight as Zn (*1*). As early as 1885 (*2*), *Thlaspi caerulescens* J. & C. Presl growing on Zn-rich soils had been observed to contain elevated concentrations of Zn. Numerous reports now exist of *T. caerulescens* containing Zn in excess of 153 μmol g^{-1} (>1% by weight) in dry shoot matter (*3*, *4*). A better understanding of the biological mechanisms involved in this hyperaccumulation would have practical implications for the development of phytoremediation (*5*)—the use of plants to remove pollutant metals from soils. For example, by facilitating the identification and transfer of genetic material from relatively small, slow-growing, wild hyperaccumulator species to high biomass, rapidly-growing, crop plants. This would allow the rational design of plants ideally suited for phytoremediation applications. Here, we report the use of X-ray absorption spectroscopy (XAS) to identify Zn chelates in vivo within different tissues of the Zn-hyperaccumulator *T. caerulescens*.

Materials and Methods

Seed Material and Analysis of Field-Collected Plant and Soil Samples. Seeds of *T. caerulescens* were collected from plants growing at an abandoned Pb mine near the Miners' Standard in Bradford Dale, Youlgreave, Derbyshire, England. Leaf samples collected from randomly selected individuals of *T. caerulescens* and other species as well as soil samples were analyzed on site. Soil samples were collected in the immediate vicinity of the roots of the plants used for leaf analysis. Plant samples were rinsed, blotted with absorbent paper, and gently dried using a portable gas cooker. Dried plant material and dry soil samples were placed in plastic vials with Mylar windows, and elemental contents were determined using a portable X-ray fluorescence analyzer (Spectrace 9000, TN Technologies, Inc.). Instrument readings were verified daily by running standards of known composition, which had been previously determined by inductively coupled plasma-emission spectroscopy (ICP). For ICP analysis (Fisons Accuris, Fisons Instruments, Inc., Beverly, MA), oven-dried plant material was digested in 5 mL of concentrated HNO_3 (trace metal grade) at 180 °C until the remaining volume of digest solution was less than 2.5 mL, then the digests were clarified by adding 1 mL of $HClO_4$ and heating to 180 °C. Certified National Institute of Standards and Technology plant (peach leaf) standards were carried through the digestion protocol and analyzed as part of the quality assurance/quality control program. Reagent blanks and spikes were used where appropriate to ensure accuracy and precision in the analysis.

Plant Growth. Seeds were germinated on filter paper moistened with 2.8 mmol L^{-1} $Ca(NO_3)_2$ for 1 week. Subsequently, 10 seedlings were transferred into 12 L of hydroponic solution. Seedlings were initially supported by moist vermiculite and later by absorbent cotton. Solutions were continuously aerated and exchanged at intervals of 7−18 days, according to plant size. The composition of all hydroponic solutions was as follows: 0.28 mmol L^{-1} Ca^{2+}, 0.6 mmol L^{-1} K^+, 0.2 mmol L^{-1} Mg^{2+}, 0.1 mmol L^{-1} NH_4^+, 1.16 mmol L^{-1} NO_3^-, 0.1 mmol L^{-1} $H_2PO_4^-$, 0.2 mmol L^{-1} SO_4^{2-}, 4.75 μmol L^{-1} ferric tartrate, 0.03 μmol L^{-1} Cu^{2+}, 0.08 μmol L^{-1} Zn^{2+}, 0.5 μmol L^{-1} Mn^{2+}, 4.6 μmol L^{-1} H_3BO_3, and 0.01 μmol L^{-1} MoO_3. Plants were cultivated in a growth chamber with 10-h light periods, with light provided by fluorescent and incandescent lamps at a light intensity of 20 800 lux. All plants were maintained at day/night temperatures of 22/22 °C and a constant humidity of 50%. After 5 weeks growth, 50 μM Zn was added to the hydroponic solution as $ZnSO_4$. Seven days after Zn exposure, plants were harvested and decapitated, and then xylem exudate was collected for 1 h. Roots and shoots were separated and rinsed in deionized water. Roots were incubated in ice cold 1 mM $Ca(NO_3)_2$ for 15 min to remove adsorbed Zn. Samples were split for both X-ray absorption spectroscopy and metal analysis and frozen in liquid nitrogen for storage at −80 °C.

X-ray Spectroscopy. Plant samples were shipped to Stanford Synchrotron Radiation Laboratory on dry ice. To minimize breakdown and mixing of cellular components within the plant material, care was taken to keep the tissue frozen at all times prior to measurement. Frozen plant tissues were carefully ground under liquid nitrogen and compacted

* Corresponding author fax: (520)523-8111; telephone: (520)523-6296; e-mail: david.salt@nau.edu.
† Northern Arizona University.
‡ Exxon Research and Engineering.
§ University of Sheffield.
∥ Rutgers University, Cook College.
⊥ Stanford Synchrotron Radiation Laboratory.

10.1021/es980825x CCC: $18.00
Published on Web 01/21/1999

FIGURE 1. ***T. caerulescens*** **growing on an abandoned Pb mine near the Miners' Standard in Bradford Dale, Youlgreave, Derbyshire, England.**

into liquid nitrogen-cooled 1 mm path length Lucite sample holders with Mylar windows. Aqueous model compounds used in the XAS edge-fitting procedure were diluted by 30−50% v/v with glycerol (to avoid ice crystal formation) before pipetting into holders and rapidly freezing in liquid nitrogen. During data collection, samples were held at a temperature of approximately 15 K using a flowing liquid helium cryostat.

X-ray absorption spectroscopy data collection was carried out on beamline 7−3 of the Stanford Synchrotron Radiation Laboratory using a Si(220) double crystal monochromator, 1 mm upstream vertical aperture, and no focusing optics. Incident intensity was measured using a nitrogen-filled ion chamber, and the absorption spectrum was collected in fluorescence using a 13-element germanium detector (*6*) by monitoring the Zn K_α fluorescence. Spectra were energy-calibrated with respect to a spectrum of Zn foil, collected simultaneously with the spectrum of each sample; the first energy-inflection of which is assumed to be 9660.7 eV.

X-ray absorption spectroscopy data reduction was carried out using the EXAFSPAK suite of programs according to standard methods (*7*). Quantitative edge-fitting analysis was performed using the program DATFIT (*8*). Here, the edge spectrum of the plant material is fit using a least-squares algorithm to a linear combination of edge spectra from a library of Zn model compounds. The fractional contribution of each model spectrum to the fit is then directly proportional to the percentage of Zn present in that form in the plant material.

Model compounds used in the edge-fitting procedure were as follows: aqueous, 6.7 mM $ZnSO_4$; zinc malate, 7.0 mM $ZnSO_4$ + 70 mM malate, pH 6.5; zinc oxalate, 7.0 mM $ZnSO_4$ + 70 mM oxalate, pH 7.0; zinc citrate, 6.7 mM $ZnSO_4$ + 27 mM citrate, pH 7.0; zinc succinate, 7 mM $ZnCl_2$ + 70 mM succinate; zinc histidine, 6.7 mM $ZnSO_4$ + 80 mM histidine, pH 7.0. All solutions were prepared in 30% glycerol to prevent ice crystal formation. Cell wall ghosts were prepared from *T. caerulescens* shoots (*10*). Shoot cell wall material was exposed to 100 μM $ZnSO_4$ in hydroponic solution for 24 h, rinsed in deionized water, and frozen in liquid nitrogen for storage.

Extended X-ray absorption fine structure (EXAFS) spectra were quantitatively analyzed using EXAFSPAK (EXAFSPAK was written by Dr. Graham N. George of SSRL, Stanford, CA) according to established procedures. Phase and amplitudes were calculated by FEFF-7 (*9*) using crystalline $(NH_4)_4Zn(Cit)_2$ (*18*) for the Zn−O shells and $Zn(Im)_4(ClO_4)_2$ (*28*) for all other shells. The threshold energy (k = 0) was initially optimized and fixed at 9672.2 eV. The interatomic distance (R) and, where appropriate, coordination number (N) were refined for each shell. A common Debye−Waller factor (σ^2) was refined for the first shells of each spectrum. For the second shell, σ^2 refined as 0.004(1) for a zinc imidazole solution spectrum and was fixed at this value for other spectra. The second shell also included a Zn−C−N−Zn multiple scattering path that was found to be significant in the imidazole solution. Three times the estimated standard deviation is shown in parentheses after the parameter.

Results and Discussion

Using a portable X-ray fluorescence analyzer (Spectrace 9000, TN Technologies, Inc, Round Rock, TX), we were able to measure, in the field, shoot Zn concentrations of 306 μmol g^{-1} dry mass ± 55 (SD, n = 5) in *T. caerulescens* growing on spoil containing 41 μmol g^{-1} ± 14 (SD, n = 5) total Zn (Figure 1). At this site, *T. caerulescens* was accumulating 35 times more Zn in shoots than other species growing nearby on the same soil, thus confirming the Zn-hyperaccumulator status of *T. caerulescens*.

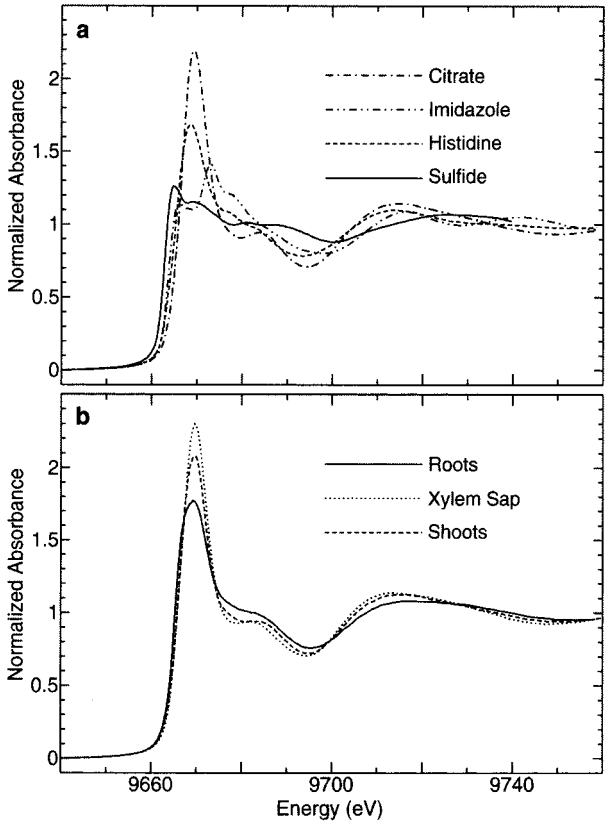

FIGURE 2. (A) Zinc K-edge X-ray absorption spectra of selected aqueous Zn species: zinc citrate (as aqueous 6.7 mM $ZnSO_4$ + 27mM citrate, pH 8), zinc imidazole (as aqueous 6.7 mM $ZnSO_4$ + 80 mM imidazole, pH 7.0), zinc histidine (as aqueous 6.7 mM $ZnSO_4$ + 80 mM histidine, pH 7.0) and sulfide (Zn rubredoxin from *Pyrococcus furiosus* (*29*)). (B) Zinc K-edge X-ray absorption spectra of root, xylem sap, and shoot of *T. caerulescens*.

The ability of *T. caerulescens* to accumulate Zn appears to be due to both enhanced Zn export to shoots and elevated Zn tolerance (*10*). The biochemical mechanisms involved are unknown, although it has been suggested that chelation of the accumulated metal by organic acids (*11, 12*) or histidine (*13*) is important. Unfortunately, most of these studies are difficult to interpret due to the possible appearance of metal complexes as an artifact of the extraction and separation processes (*14*).

In an effort to overcome these problems, we have used X-ray absorption spectroscopy to probe the coordination geometry of metals in plants with minimal tissue disturbance (*15, 13, 16*). The Zn X-ray absorption edge is sensitive to the molecular environment, as demonstrated clearly in the edge spectra of zinc histidine and zinc citrate (Figure 2A). In the presence of excess histidine and at neutral pH, Zn is coordinated by both neutral ring and amino nitrogens and by the weakly interacting negative carboxyl oxygen to form the complex $Zn(His)_2$ (*17*). In contrast, citrate coordinates Zn through the hydroxyl and carboxyl oxygens (*18*). These differences in the coordination geometry of Zn between the two chelates produce large differences in their X-ray absorption edge spectra (Figure 2A).

By comparing the Zn K-edge X-ray absorption spectra of root, xylem sap, and shoot of *T. caerulescens* (Figure 2B) with the spectra of standard compounds, we were able to obtain information on the likely identity of the endogenous Zn chelates in these tissues (*19*) (Figure 3). In the roots, the majority of the intracellular Zn was coordinated with histidine, with the rest complexed to the cell wall (Table 1). Zinc appeared to be transported to the shoot in the xylem

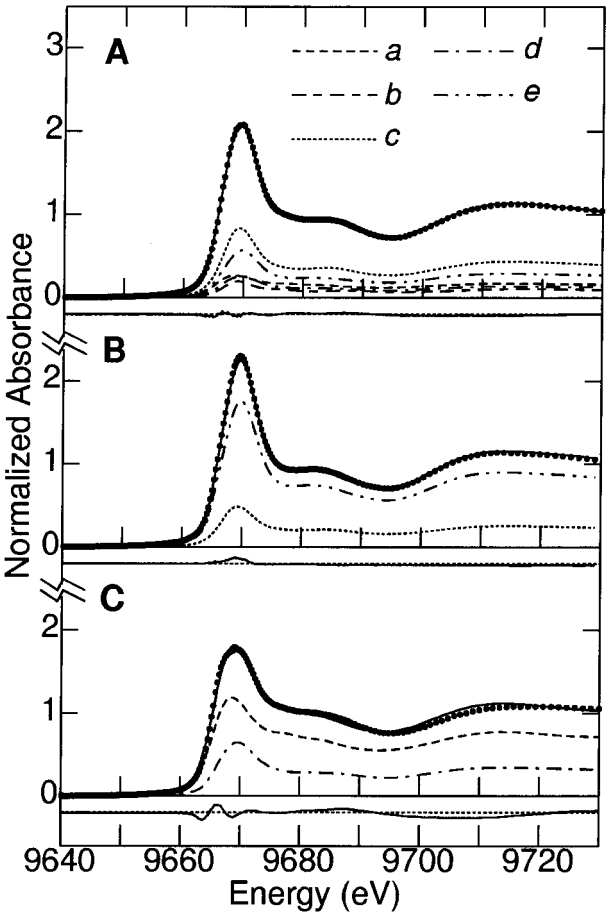

FIGURE 3. Results of quantification of Zn K-edge X-ray absorption spectra of shoots (A), xylem sap (B), and roots (C) of *T. caerulescens*. The spectrum of a mixture of species is the sum of the spectra of individual species scaled by their relative fractions. By fitting spectra of various model Zn complexes to the data (solid circles), we were able to determine their fractional contribution to the spectra collected from the sample. Model Zn complexes used in the fit: histidine (a), oxalate (b), citrate (c), cell wall ghosts (d), and aqueous Zn (e). The solid line underneath each plot represents the residual data not fit by the model. Data from these fits are presented in Table 1.

TABLE 1. Distributions of Zn Species in *T. caerulescens* Tissues

Zn species	root[a]	shoot[a]	xylem sap[b]
total Zn	20.3	77.7	1.1
	percent speciation (%)		
aqueous	0	26	79
malate	0	0	0
citrate	0	38	21
succinate	0	0	0
oxalate	0	9	0
histidine	70	16	0
cell wall	30	12	0
goodness of fit[c]	0.897×10^{-3}	0.096×10^{-3}	0.297×10^{-3}

[a] Units: μmol g^{-1} dry biomass. [b] Units: mM. [c] The goodness of fit is defined as $\sum[(I_{obsd} - I_{calcd})^2]/n$, where n is the number of points in the spectrum and I_{obsd} and I_{calcd} are the observed and calculated points, respectively. A lower goodness of fit represents a better match between the fitted model spectra and the sample spectrum.

mainly as a hydrated cation, with chelation by citrate playing a small role (Table 1). In the shoots, Zn coordination was

TABLE 2. Results of EXAFS Curve-Fitting Analysis of Zn-Enriched *T. caerulescens* Tissues and Various Zn Model Compounds

	first coordination shell		second coordination shell
sample	***N* type at *R* (Å)**	**σ^2 (Å^2)**	***N* type at *R* (Å)**
whole-root tissue	3.3(6) Zn−N at 1.99(1) 2.7(4) Zn−O at 2.11(1)	0.003(2)	3.1(9) Zn···C at 2.98(2)
xylem sap	6.5(6) Zn−O at 2.082(4)	0.008(1)	
whole-leaf tissue	5.5(4) Zn−O at 2.068(3)	0.008(10)	
zinc histidine	3.8(9) Zn−N at 2.08(2) 1.1(4) Zn−O at 2.23(6)	0.005(2)	3.8(9) Zn···C at 3.03(2)
zinc citrate	5.9(6) Zn−O at 2.077(5)	0.007(1)	
aqueous Zn^{2+}	6.3(5) Zn−O at 2.082(4)	0.001(1)	

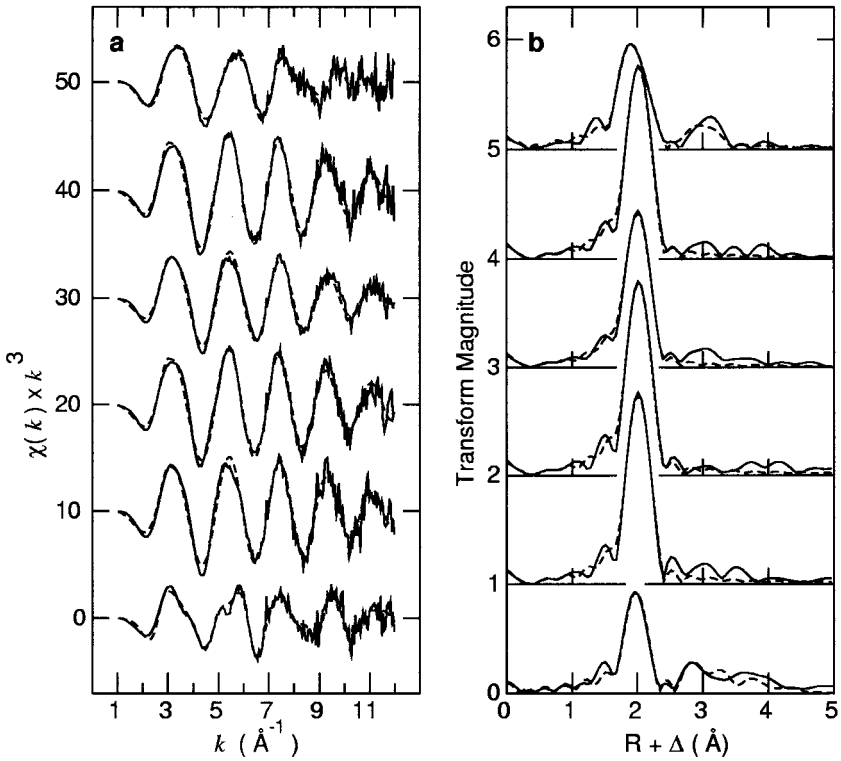

FIGURE 4. Zinc K-edge EXAFS (A) and corresponding Fourier transforms (B) for Zn-enriched *T. caerulescens* tissues and Zn solution model compounds. Solid lines represent the data, and dashed lines the results of the fits of Table 2. Top to bottom: whole-root tissue, xylem sap, whole-leaf tissue, aqueous Zn^{2+}, zinc citrate, zinc histidine. Fourier transforms have been phase-corrected for the first shell.

dominated by citrate with smaller contributions from hydrated zinc, histidine, cell wall, and oxalate binding (Table 1).

Zinc K-edge extended X-ray absorption fine structure (EXAFS) analysis allows determination of both interatomic distances and coordination numbers for metal complexes. Using EXAFS analysis, we determined that Zn in roots of *T. caerulescens* has two first coordination shells, fitted as nitrogen and oxygen at 1.99 and 2.11 Å, respectively (Table 2). The presence of a second coordination shell at 2.98 Å with multiple scattering is consistent with interactions from the heterocyclic histidine ring (Figure 4, Table 2). This second coordination shell is not seen in shoot or xylem sap (Figure 4). Coordination of Zn by two different nearest neighbor atoms and the presence of a next nearest carbon atom appear diagnostic for Zn coordinated with histidine. The difference in Zn−N bond lengths between the roots and the $Zn(His)_2$ solution species is relatively large at 0.09 Å. However, a search of the Cambridge Structural Data Base reveals that both distances are within the expected range for Zn−N(His) coordination of 1.97−2.10 Å.

Xylem sap Zn was found to be coordinated with six oxygen atoms at a bond length of 2.082 Å, an identical coordination to that seen in an aqueous solution of $ZnSO_4$ (Table 2). In shoots, the Zn−O bond length was slightly shortened to 2.068 Å with a coordination number of 6, consistent with aqueous zinc citrate (Table 2).

Accumulation of Zn in *T. caerulescens* shoots requires Zn transport across the cytoplasm of root cells and translocation in the xylem to the shoots (*20*). Due to the high stability constant of the zinc histidine complex and the protonation constants of histidine, this amino acid is an ideal chelator of Zn at the pH values commonly found in the cytoplasm (pH ~7.5). However, at the low pH values of the xylem sap (pH ~5.5), the imidazole nitrogen of histidine becomes protonated, which results in a decrease of the apparent stability constant of the zinc histidine complex, favoring the coordination of Zn by water and organic acids including citrate. These are the forms in which Zn moves to shoots. The change in Zn speciation in the xylem sap can be clearly seen in the edge spectra (Figure 2B).

Cellular Zn is known to be preferentially accumulated within vacuoles in the leaves of a number of different plant species including tobacco, barley, and *T. caerulescens* (*21*−*23*), and this has been proposed as a possible mechanism of zinc tolerance in plants (*12*, *24*). Zinc accumulation within

the vacuole, as a Zn detoxification mechanism, is also supported by the observation that the vacuolar volume fraction of meristematic cells of *Festuca rubra* increases during Zn exposure (*25*). Organic acids are also known to accumulate in plant vacuoles (*26*), and chelation of Zn in the vacuole by certain organic acids, particularly citrate, is favored by the low pH (∼5.5) of this organelle (*27*). Our observation that Zn is coordinated by citrate in the leaves of *T. caerulescens* (Table 1) supports the hypothesis that Zn is accumulated in *T. caerulescens* leaves as a citrate complex in the vacuole. This supports the earlier contention that vacuolar localization of Zn is involved in Zn resistance in *T. caerulescens* (*23*).

In this study, we have obtained the first direct measurements of the in vivo speciation of Zn in the Zn-hyperaccumulator *T. caerulescens*. Our data are consistent with the hypothesis that histidine acts to transport Zn within cells and that organic acids act to coordinate Zn during long-distance transport and storage.

Acknowledgments

The authors extend their appreciation to Graham George for his help with XAS data collection and to John MacDonald for his help in searching for relevant crystal structures. This research was partially supported by a grant from the U.S. Department of Energy to D.E.S. and by Phytotech Inc. SSRL is funded by DOE BES. The SSRL Biotechnology Program is supported by NIH NCRR, Biomedical Technology Program; further support is provided by DOE OBER.

Literature Cited

(1) Baker, A. J. M.; Brooks, R. R. *Biorecovery* **1989**, *1*, 81−126.
(2) Baumann A. *Landwirtsch. Vers.-Stn.* **1885**, *31*, 1−53.
(3) Reeves, R. D.; Brooks, R. R. *J. Geochem. Explor.* **1983**, *18*, 275−283.
(4) Baker, A. J. M.; Reeves, R. D.; Hajar, A. S. M. *New Phytol.* **1994**, *127*, 61−68.
(5) Salt, D. E.; Smith, R. D.; Raskin I. *Annu. Rev. Plant Physiol. Plant Mol. Biol.* **1998**, *49*, 643−668.
(6) Cramer, S. P.; Tench, O.; Yocum, M.; George, G. N. *Nucl. Instrum. Methods Phys. Res.* **1988**, *A266*, 586−591.
(7) Koningsberger, D. C.; Prins, R. *X-ray Absorption Principles, Applications, Techniques of EXAFS, SEXAFS and XANES*; John Wiley and Sons: New York, 1988.
(8) George, G. N.; Gorbaty, M. L.; Keleman, S. R.; Sansone, M. *Energy Fuels* **1991**, *5*, 93−97.
(9) Rehr, J. J.; Zabinsky, S. I.; Albers, R. C. *Phys. Rev. Let.* **1992**, *69*, 3397−4000.
(10) Lasat, M.M.; Baker, A. J. M.; Kochian, L. V. *Plant Physiol.* **1996**, *112*, 1715−1722.
(11) Reeves, R. D. *The vegetation of ultramafic (serpentine) soils*; Baker, A. J. M., Proctor, J., Reeves, R. D., Eds.; Intercept Ltd.: Andover, U.K., 1992; pp 253−277.
(12) Mathys, W. *Physiol. Plant.* **1977**, *40*, 130−136.
(13) Krämer, U.; Cotter-Howells, J. D.; Charnock, J. M.; Baker, A. J. M.; Smith, J. A. C. *Nature* **1996**, *379*, 636−638.
(14) Farago, M. E.; Mahmoud, I.; Clark, A. J. *Inorg. Nucl. Chem. Lett.* **1980**, *16*, 481−484.
(15) Salt, D. E.; Prince R. C.; Pickering, I. J.; Raskin, I. *Plant Physiol.* **1995**, *109*, 1427−1433.
(16) Salt, D. E.; Pickering, I. J.; Prince, R. C.; Gleba, D.; Dushenkov, S.; Smith, R. D.; Raskin, I. *Environ. Sci. Technol.* **1997**, *31*, 1635−1644.
(17) Kistenmacher, T. J. *Acta Crystallogr.* **1972**, *B28*, 1302−1304.
(18) Swanson, R.; Isley, W. H.; Stanislowski, A. G. J. *Inorg. Biochem.* **1983**, *18*, 187−194.
(19) Pickering, I. J.; Brown, G. E.; Tokunga, T. K. *Environ. Sci. Technol.* **1995**, *29*, 2456−2459.
(20) Marschner, H. *Mineral nutrition of higher plants*; Academic Press: London, 1995.
(21) Krotz, R. M.; Evangelou, B. P.; Wagner, G. J. *Plant Physiol.* **1989**, *91*, 780−787.
(22) Brune, A.; Urbach, W.; Dietz, K.-J. *Plant Cell Environ.* **1994**, *17*, 153−162.
(23) Vázquez, M. D.; Poschenrieder, Ch.; Barceló, J.; Baker, A. J. M.; Hatton, P.; Cope, G. H. *Bot. Acta* **1994**, *107*, 243−250.
(24) Brookes, A.; Collins, J. C.; Thurman, D. A. *J. Plant Nutr.* **1981**, *3*, 695−705.
(25) Davies, K. L.; Davies, M. S.; Francis, D. *Plant Cell Environ.* **1991**, *14*, 399−406.
(26) Ryan, C. A.; Walker-Simmons, M. *Methods Enzymol.* **1983**, *96*, 580−589.
(27) Wang, J.; Evangelou, B. P.; Wagner, G. J. *Plant Physiol.* **1992**, *99*, 621−626.
(28) Bear, C. A.; Duggan, K. A.; Freeman, H. C. *Acta Crystallogr.* **1975**, *B32*, 2713−2715.
(29) George, G. N.; Pickering, I. J.; Prince, R. C.; Zhou, Z. H.; Adams, M. W. *Biol. Inorg. Chem.* **1996**, *1*, 226−230.

Received for review August 13, 1998. Revised manuscript received November 25, 1998. Accepted December 3, 1998.

ES980825X